Open Research Online

The Open University's repository of research publications
and other research outputs

Simulating and reproducing instrument background for x-ray CCD spectrometers in space

Conference or Workshop Item

How to cite:

Hall, David; Holland, Andrew and Turner, Martin (2008). Simulating and reproducing instrument background for x-ray CCD spectrometers in space. In: Proceedings of SPIE: High Energy, Optical, and Infrared Detectors for Astronomy III, 23-27 Jun 2008, Marseille.

For guidance on citations see FAQs.

Version: Accepted Manuscript

Link(s) to article on publisher's website:
http://dx.doi.org/doi:10.1117/12.790711

oro.open.ac.uk

Simulating and reproducing instrument background for X-ray CCD spectrometers in space

David Hall[*a], Andrew Holland[b] and Martin Turner[c]

[a] Imaging for Space and Terrestrial Applications, School of Engineering and Design,
Brunel University, Uxbridge, Middlesex, UB8 3PH, UK
[b] Planetary and Space Sciences Research Institute, Open University,
Walton Hall, Milton Keynes MK7 6AA
[c] Space Research Centre, University of Leicester,
University Road, Leicester LE1 7RH, UK

ABSTRACT

In anticipation of the European Space Agency (ESA) X-ray Evolving Universe Spectroscopy (XEUS) mission, designed as a follow-on to the ESA X-ray Multi Mirror (XMM-Newton) mission, the instrument background for the XMM-Newton mission, the Japanese Space Agency Suzaku mission and the NASA Swift mission has been studied. The instrument background has been modelled using the Geant4 toolkit to establish the constituent components for the differing orbits and detector designs across the energy range from 1 keV to 12 keV. The results, consistent with the spectra obtained in-orbit, are then discussed. With knowledge of the dominant components of the instrument background, methods targeted at reduction in future missions are considered, with experimental results designed to determine their effects.

Keywords: Instrument background, XMM, Suzaku, Swift, XEUS, Geant4, CCD X-ray spectrometer.

1. INTRODUCTION

X-ray CCD spectrometers for use in space applications, as with all devices, experience some degree of background signal. At ground level, the dominant sources of background in a CCD are generally the dark current and the readout/system noise. These well understood sources of background are negligible compared with the sources of background experienced in orbit. In orbit, the dominant sources of background in an X-ray CCD spectrometer are the unresolved Cosmic X-ray Background (CXB) and the instrument background.

Through examination of the background spectra of several missions, one can hypothesise as to the causes of the background. Without an in depth study, the resulting differing views cannot be fully justified. Here, the simulation toolkit Geant4 has been used to replicate the conditions experienced by the detectors in orbit. Through a Monte-Carlo simulation technique the individual components of the background have been investigated, providing the building blocks for a better understanding.

The three missions selected for analysis were chosen to allow comparisons to be drawn between the detector design and the orbit of the mission. The XMM-Newton and Swift missions both use the same type of MOS CCD and therefore allow the effect of the mission orbit to be studied. The Swift and Suzaku missions use different types of detectors and allow the effects of the detector design to be investigated at a similar orbit. Through these simulations a more detailed understanding of the background can be acquired.

Of the two main sources of background the CXB is currently the better understood [3]. The concentration in this study is on the production of the instrument background, namely the flat continuum seen in all three missions. The characteristic X-ray fluorescence peaks, due to the material placed around the detector, are believed to be well understood and as such, these are not modelled here.
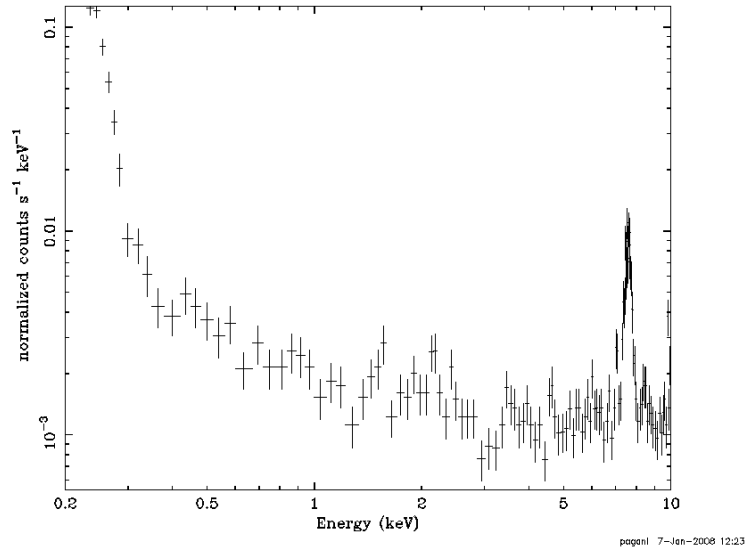
2. INSTRUMENT BACKGROUND

The background is formed by two dominating components: the Cosmic X-ray Background (CXB) and the instrument background. Figure 1 shows a simplified graphic of the background, using data taken from [3]. From this diagram the relative dominance of the two components can be seen and it is clear that the instrument background dominates above a few keV.
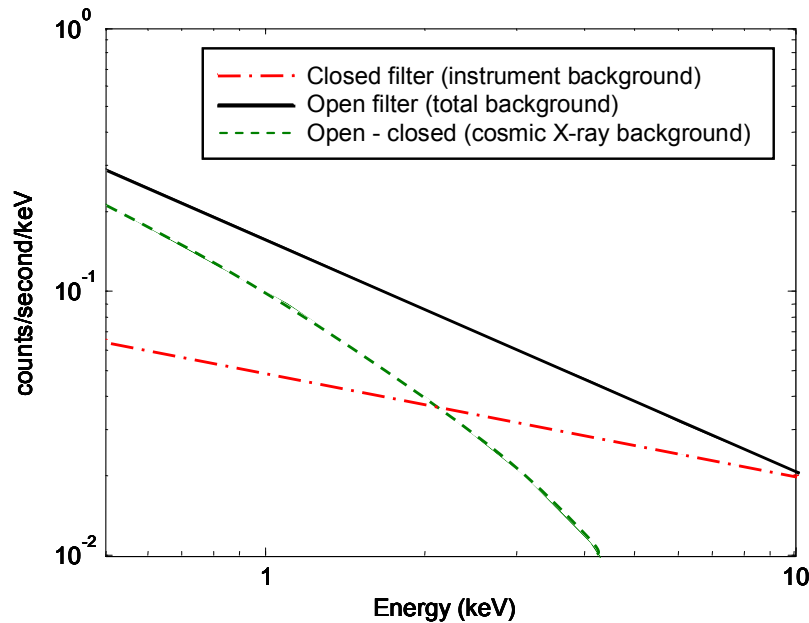

Figure 1. The Instrument background is taken with the closed filter. The total background is taken with the open filter. The difference between these components therefore gives the Cosmic X-ray Background (CXB). The CXB dominates below 2 keV. Above 2 keV the instrument background dominates. Data taken from [3] for the XMM-Newton MOS1 X-ray CCD camera.

The instrument background arises from interactions of high energy particles with the detector and surrounding material. The orbit of the detector has a large impact on the incident spectrum of particles and one would therefore expect the instrument background to be dependent on the orbit of the mission. The primary particles are those which are incident on the outside of the detector shielding, some of which may pass through the shielding to the detector. The secondary particles are those which arise from the interactions of the primary particles with the material surrounding the detector. The way in which the primary and secondary particles interact with the CCD is dependent on the detector design.

The instrument background from these three missions can be seen to vary with both the orbit and the detector design. Figure 2 shows an example of a spectrum used in the analysis, provided by Claudio Pagani at Penn State University. The spectral continuum has been reproduced mathematically for all three missions, Figure 3, to allow numerical comparisons to be made and to allow a more accurate comparison with the simulated data. The forms of the continua have been examined and the results proposed from this study are discussed below. The data files for these spectra have been provided by Andrew Read (Leicester University), Claudio Pagani (Penn State University) and with reference to [1] and [8].

Figure 2. The instrument background for the Swift XRT. This dataset was collected in September 2007 when pointing accuracy was lost. With the XRT pointing too close to the Sun the XRT Sun shutter was forced to close. The shutter was re-opened two days later, during which time the dataset collected was purely instrumental background. The dataset here was taken for a region of interest (ROI) set as a circle with a radius 200 pixels and then corrected for bad columns (pixel size of 40 μm side).
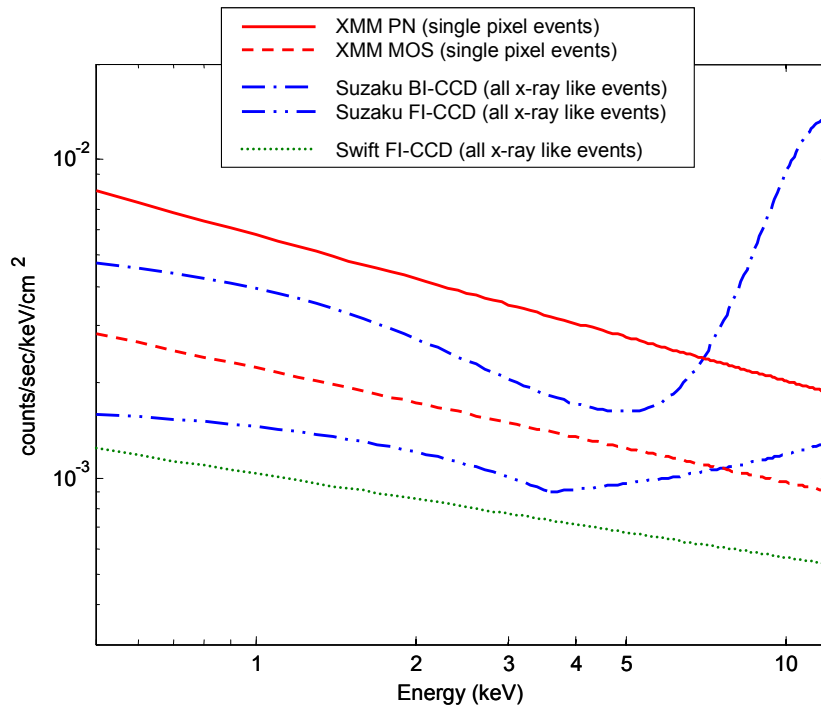
Figure 3. The in-orbit spectral continua for the three missions, scaled for direct comparison (as with Figure 2, but given here per cm^2).

3. GEANT4 SIMULATION

The Geant4 toolkit allows the user to independently code all aspects of the simulation. The code is then compiled with reference to the toolkit which provides the physical aspects such as the interactions and energy loss.

In this study it is the particles arriving at the CCD which are the most important. In order to simplify the simulation and provide shorter run-times, the surroundings to the detector were modelled as a spherical aluminium shell of thickness 3 cm. The effect of such an approximation has previously been studied [6]. A more realistic model was created for the Suzaku XIS detector and the particles reaching the detector were simulated. A second model, using the aluminium shell as an approximation, was then examined. The differences between the two spectra detected at the CCD were declared negligible. The second simulation was found to take substantially less computational time due to the simplified particle tracks in the aluminium shell.

3.1 The detectors

The XMM-Newton mission contains two types of X-ray detectors: the MOS CCD and the pn-CCD. The pn-CCD can be compared to a back-illuminated CCD for the purposes of this study, as it is the interaction of incoming particles in the silicon of the detector which is of greatest importance.

The Swift XRT uses the same MOS CCD as that found in the XMM-Newton mission (the e2v CCD-22). As the Swift and XMM-Newton missions contain the same detector type, the effect of the orbit on the instrument background can be isolated.

The Suzaku mission contains two types of X-ray CCD detectors: the Front-Illuminated CCD (XIS0, XIS2 and XIS3) and the Back-Illuminated CCD (XIS1).

In the simulation, the detectors were created with the layers shown in Table 1. The simulated detectors are formed as a collection of pixels, each of which is sensitive to incident radiation. If energy is deposited inside a pixel the details of the particle and the energy deposited are recorded. The particle details recorded include the particle type, the depth of the interaction in the silicon and details of the origins of the particle. The origin of the particle gives the details as to whether the particle is a primary, such as a proton passing through the shielding and on through the detector, or a secondary particle. If the particle is found to be a secondary particle then the details of the parent particle and the interactions leading to the production of the particle are recorded. From this record, each particle can be traced and the results of the simulation can be analysed using bespoke code.

Aside from the thickness, the main difference between the MOS CCD and pn-CCD is the surface structure. For this reason the structure of the MOS electrodes has been more accurately modelled and a PCB layer has been added to the pn-CCD detector. The electrode structure for the MOS CCD was modelled with the layers shown in Table 2.

Table 1. The four detector types are modelled using the data shown here. Particles can interact with all parts of the detector, but the *sensitive detector* is the region in which the energy loss of a particle is recorded. The similarities between the MOS-CCD/FI-CCD and pn-CCD/BI-CCD are seen here.

Layer	MOS CCD	pn-CCD	FI	BI
Electrode structure	1 μm	-	0.7μm	-
Si sensitive detector	30 μm	300 μm	70 μm	45 μm
Si field-free region and substrate	600 μm	-	605 μm	-
Cu layer (on PCB)	-	100 μm	-	-
Pixel size	40 μm	150 μm	24 μm	24 μm

Table 2. The more accurate model of the MOS electrodes.

Layer	MOS	Fraction of surface covered
SiO_2	0.5 μm	0.6
Si	0.5 μm	0.6
Si_3Ni_4	0.085 μm	0.6
SiO_2 layer	0.085 μm	1

3.2 The orbits

The differences in the instrument background spectra found at the different orbits are due to the differing incident particle spectra. The Highly Elliptical Orbit (HEO) of the XMM-Newton mission provides a substantially different incident particle spectrum to that of the two Low Earth Orbit (LEO) missions, Swift and Suzaku. This has a major impact on the instrument background.

The XMM-Newton mission has a HEO with a perigee of approximately 7 000 km and an apogee of 120 000 km. At this orbit, ionised nuclei dominate the galactic cosmic ray spectrum (dominated by approximately 95% protons). These high energy protons leave an easily recognisable trace in the CCD. By counting these interactions, the flux of protons through the detector has been estimated at 2-2.5 protons cm^{-2} s^{-1} [4]. This was found to be consistent with a rate of 4.4 cm^{-2} s^{-1} in solar minimum conditions reduced by a factor of two at solar maximum due to solar modulation.

The Suzaku mission has a low-earth-orbit (LEO) of approximately 570 km, where the cosmic-ray spectrum is dominated by protons, electrons and photons. The term photon will be used here as opposed to X-ray or gamma ray as the simulation works on a particle by particle basis. At this lower orbit it cannot be assumed that protons have the dominant impact on the instrument background. Through preliminary testing of the system the energy windows of the cosmic-ray spectrum were selected. The low energy cut-off was set such that the particles have sufficient energy to pass through the aluminium shielding. The spectrum was devised using data from [5] and [6]. Due to complications in accurately simulating the full spectrum of particles (similar to those found in earlier studies [6]) each particle type was simulated individually and the form of the spectrum examined independently. With reference to the in-orbit spectrum it is then possible to piece together the results of the simulation and to propose a theoretical response of the CCDs at LEO. A brief summary of the incident particle spectra is shown in Table 3.

Table 3. A summary of the incident particle spectra at the two orbits: LEO and HEO. Data for LEO taken from [5] and [6]. The table shows the approximate energy ranges considered (flux given in brackets, counts per second per cm^2 per MeV per sr).

Orbit	Missions	Particle	Details
HEO	XMM- Newton	Proton	2.25 protons cm^{-2} s^{-1}, simple power law from 100 MeV to 400 MeV (normalised to proton flux).
LEO	Swift Suzaku	Proton	0.6 protons cm^{-2} s^{-1}, simple power law from 70 MeV (10^{-4}) to 700 MeV (10^{-5})
		Electron	Simple power law from 10 MeV (10^{-3}) to 200 MeV (10^{-4})
		Photon	Simple power law from 10 keV (10^4) to 200 keV (10^0)

The Swift mission has a low earth orbit similar to that of the Suzaku mission at approximately 600 km. The proton flux at LEO was found to be 0.6 protons cm^{-2} s^{-1} [6]. Using this flux as a normalising factor the instrument background of the Swift and XMM-Newton MOS detectors can be compared.

Each particle which is incident on the system is created at a random position on the outer surface of the aluminium shell. The particle is then directed towards another random position on the surface of the aluminium shell. This provides random positions and directions uniformly distributed on the surface of the aluminium shell. Projecting the primary particles radially onto the shell does not account for all possible secondary particles. The flux of the incident particles can then be normalised to the appropriate level using the proton counting method described above.

3.3 Data collection

Details of energy deposition were recorded from the regions of the simulation which were nominated as *sensitive detectors*. A selection of particle properties were recorded for each particle depositing energy in the CCD, thus enabling each particle to be traced. The data was then analysed using bespoke code to allow full control over the analysis. Using this method it is possible to differentiate between the different types of interaction and the particles involved. The interactions leading to the production of any detected secondary particles were also recorded.

The incident particle flux was normalised to the values stated previously for the two orbits. The proton flux in the simulated CCD detector was extracted using the bespoke code. The effects of these protons can be seen in the example output from the simulation shown in Figure 4. The higher energy linear tracks show the protons passing through the CCD.

Once the events have been restricted to those in the energy range required (lower than 20 keV) the events can be narrowed down to only those which are X-ray-like (those which are indistinguishable from X-rays). The grading system used to select these events was taken from the Suzaku mission ASCA Grade system. This system has been used to split the results into two classes: single pixel events and all X-ray-like events. Care must be taken when making a direct comparison between results. Due to the availability of reliable in-orbit instrument background spectra some events are given as single pixel events only and some as all X-ray-like events. All comparisons detailed here are between events of the same class type.
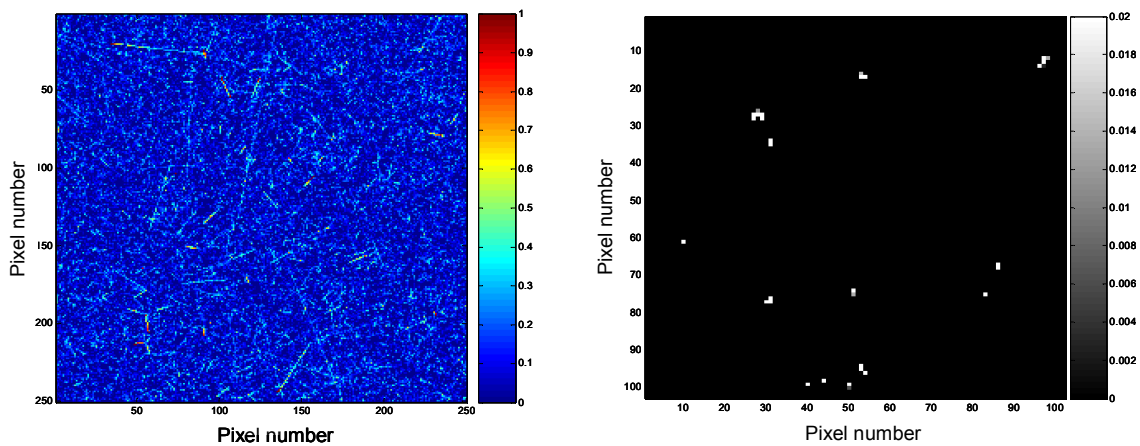

Figure 4. Two representations of a sample frame from the simulation. The left image shows all events, in which the higher energy tracks (due to protons) can be clearly seen. The right image shows the energy restricted to 0-20 keV where the different ASCA grade event types can be seen. Under these conditions it is then possible to extract X-ray-like events.

4. RESULTS

It is first necessary to discuss the particles emerging from the inner surface of the aluminium shell following bombardment with a simplified spectrum of high energy protons (100 – 400 MeV). When a proton passes through the aluminium shell, many electrons are ejected along the proton path. Each electron has an energy of a few keV and hence has a very short stopping distance in the aluminium. There is a negligible effect on the proton energy (several hundred MeV) over these distances. The majority of the ejected electrons are reabsorbed in the aluminium. The electrons ejected within a small distance of the inner surface of the aluminium shell can escape and travel onwards, with some inevitably travelling towards the CCD. With the Geant4 simulation these electrons are recorded as secondary particles from a parent primary proton. They are also recorded as particles created by hadronic low energy ionisation. The shape of the spectrum of these electrons was recorded using a sensitive detector in the form of a thin spherical shell placed directly inside the aluminium shell. This region was given the properties of a vacuum to avoid contamination of the results by further interactions. Particles were recorded as they passed through this region. These electrons of only a few keV can be absorbed within a small thickness of silicon and so all the energy can be assumed to be deposited at the point of interaction in the CCD. This means that the energy of the electron itself is the energy of the event detected in the CCD. The spectrum of electrons is shown in Figure 5, rescaled by a constant factor to allow comparison with the in-orbit XMM-Newton instrument background. This shows that it is highly possible that the instrument background is produced by these *knock-on* electrons.

It is unfortunately not the case that all these electrons are detected by the CCD. The solid angle of the CCD from the aluminium surface covers only a small fraction of possible electron trajectories from any point. The electrons may also interact in different ways with the different detector types. For this reason, the CCD is introduced to the system as detailed in Table 1 and Table 2.

Following the simulation of the XMM-Newton detectors the analysis of the results leads to some reassuring conclusions when compared with the initial results detailed above. For both detectors, approximately 97% of the single pixel events are the result of electrons formed by the process described above – the *knock-on* electrons. Examining the data in more detail, the positions of interaction of these electrons in the silicon can be determined. These electrons, as expected, are detected within a few microns of the surface of the silicon (the sensitive detector, see Table 1). The remaining 3% of events were caused by Compton scattered electrons and by the direct detection of photons produced by bremsstrahlung interactions in the aluminium shell.
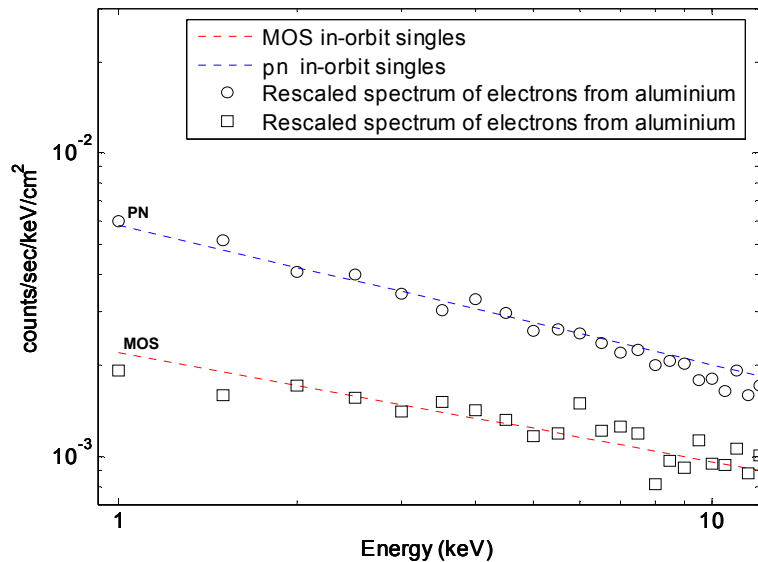
Figure 5. Spectrum of knock-on electrons emerging from the inner surface of the aluminium shell following bombardment with the incident protons. The spectrum has been rescaled to match that of the pn-CCD and MOS CCD cameras in order to compare the spectral form.

The knock-on electrons clearly appear to dominate the instrument background. It is therefore the interactions at the surfaces of the devices which seem to be of greatest importance. Examining the surface structures of the two devices (the MOS CCD and the pn-CCD) there are several clear differences. The first is the pixel size. To examine this further, a second simulation was carried out with a pn-CCD with the pixel size matching that of the MOS. Any differences in the spectra between the two pixel sizes were negligible. This implies that at the flux shown here the probability of two events occurring in the same pixel is still very slim. The second difference between the devices is the illumination position: whether the device is front-illuminated or back-illuminated.

Examining the surface structures of the devices leads to some very interesting results. Electrons passing onto the upper surface of the pn-CCD can be detected with negligible absorption before interaction. With the MOS CCD, some of the energy of these electrons can be absorbed in the electrode structure. Even with the open electrode design (Table 2) this can still act to lower the instrument background.

Looking now towards the rear of the devices one would expect similar conclusions to be drawn. The silicon substrate of the MOS CCD device can absorb these electrons meaning that they will not be detected. Any electrode-like structure on the rear of the pn-CCD will also absorb some of the energy of any electrons generated in the copper PCB layer. The electrons from the aluminium shell will be blocked by the PCB layer on the rear side of this device.

Combining the effects of the front and rear structures of the two device types leads to the conclusion proposed here: the surface structures cause the differing levels of instrument background between the two devices (the MOS CCD and the pn-CCD) and it is the knock-on electrons which dominate the instrument background for XMM-Newton (HEO).

The spectral form of the results used to arrive at this conclusion are shown in Figure 6. Approximately 1000 randomly positioned and randomly directed protons were required to simulate one second of data ($\sim$ 2-2.5 protons cm^{-2} s^{-1} at the CCD), leading to long run-times for the simulation but achieving the desired results.
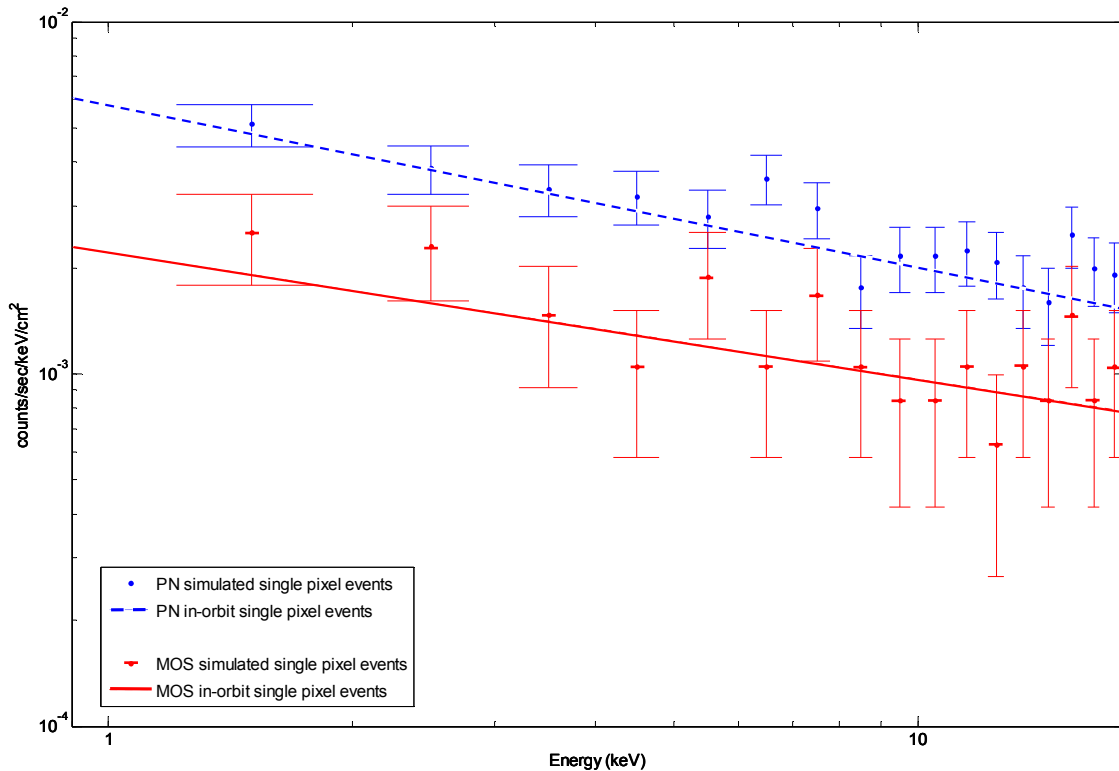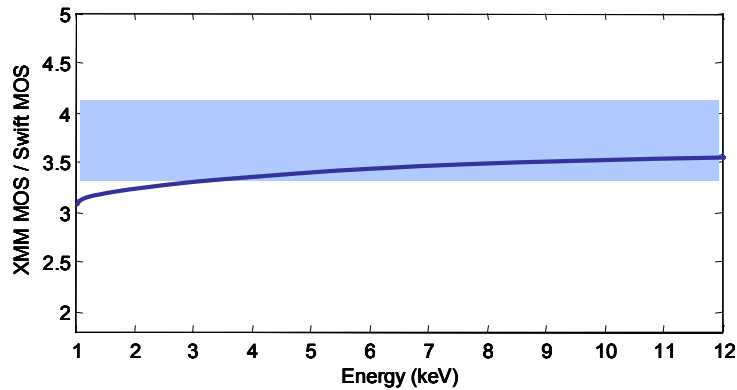

Figure 6. The spectra from the Geant4 simulation for the more accurate model of the devices (data points), binned per keV and given per second per keV per cm^2, is shown with the in-orbit continua approximations (broken lines).

With these results in mind, it is now worth considering the Swift MOS detector. If, as proposed above, the knock-on electrons are the dominant source of the instrument background, then one could reasonably expect the instrument background to scale with the incident flux of protons. At the orbit of Swift, the proton flux through the CCD was determined to be 0.6 protons $cm^{-2} s^{-1}$ [6]. This would imply an incident proton flux ratio between HEO and LEO as shown in equation 1, between 3.3 and 4.2. Taking the simplified in-orbit spectral continua, as shown previously in Figure 3, the ratio of the instrument background for the two MOS CCDs can be shown, Figure 7.

$$\text{ratio of proton flux} = \frac{\text{HEO proton flux}}{\text{LEO proton flux}} = \begin{array}{l} \dfrac{2 \text{ protos cm}^{-2} \text{ s}^{-1}}{0.6 \text{ protos cm}^{-2} \text{ s}^{-1}} = 3.3 \text{ minimum} \\[3mm] \dfrac{2.5 \text{ protos cm}^{-2} \text{ s}^{-1}}{0.6 \text{ protos cm}^{-2} \text{ s}^{-1}} = 4.2 \text{ maximum} \end{array} \qquad (1)$$

Figure 7. The ratio between the XMM-Newton MOS instrument background and the Swift MOS instrument background, allowing a comparison of the same detector under differing incident proton flux. The shaded region shows the approximate proton flux ratio between the two orbits.

The results of Figure 7 agree on the whole with this hypothesis. The ratio of the in-orbit instrument background fits with the ratio of the proton flux above approximately 4 keV. An increase in the Swift instrument background lowers the ratio between XMM-Newton and Swift. At the lower energy end of the spectrum the Swift instrument background increases above that which would be expected by a purely knock-on electron dominated spectral form. There is therefore another factor contributing at lower energies at LEO. The different incident flux of photons and electrons at LEO can help to explain this.

It is useful now to introduce the results for the simulation of the Suzaku mission. The spectral form from the incident protons has been described above for the XMM-Newton and Swift missions. Similar results were found for the Suzaku mission, with the surface structures of the devices (the presence of an electrode structure and the field-free/substrate regions) giving the same trends as seen for XMM-Newton.

The incident charged particles (primarily the electrons in this case) yielded interestingly pronounced results in the Suzaku detectors. The charged particle tracks in the CCDs caused by these particles were not fully rejected in the ASCA Grade system. When passing through the silicon of the detector, a minimally ionising charged particle will deposit a few hundred eV of energy per μm of silicon traversed (approximately 300 eV μm^{-1}). The peak in the spectrum implied by the thickness of the pn-CCD (300 μm) is approximately 90 keV. This is well out of the range of interest of the spectra studied here, and hence has negligible effect on the results. The MOS and FI-CCDs are formed by the sensitive detector layer on the upper surface and the field-free/substrate region at the lower surface. Any signal electrons due to energy deposited in the lower regions of the CCD will spread over several pixels and hence the majority of these events will be discounted: they will not fit an X-ray-like grade. For the Suzaku BI-CCD the results were somewhat different. The BI

detector consists of a 45 μm thick sensitive layer. For this thickness of silicon, a peak in the spectrum for minimally ionising charged particles can be predicted at approximately 13 keV. This peak can be seen in the in-orbit spectrum and has been reproduced in the simulation to verify the theory, Figure 8. With the peak falling within the energy range of interest the contribution to the Suzaku BI-CCD instrument background is prominent.

The results from the incident photons were less clear, but appear to give a spectral form as shown in the diagrammatic representation in Figure 9. These interactions were caused by Compton scattered electrons in the silicon of the CCD. Combining the results for all particles and separating them by interaction type the diagrammatic representation shown in Figure 9 is proposed, using the Suzaku BI-CCD as an example where all three major components are present.

Referring back to Figure 7, the apparent discrepancy between the proton flux ratio and the two MOS CCD in-orbit spectra can now be resolved. The Swift MOS instrument background in-orbit is slightly higher at lower energies than would be expected if it were purely dominated by knock-on electrons. At LEO the flux of photons is more prominent relative to the proton flux than at HEO, leading to a higher Compton scattered electron component in the CCD. This may account for the difference in the ratio at lower energies.
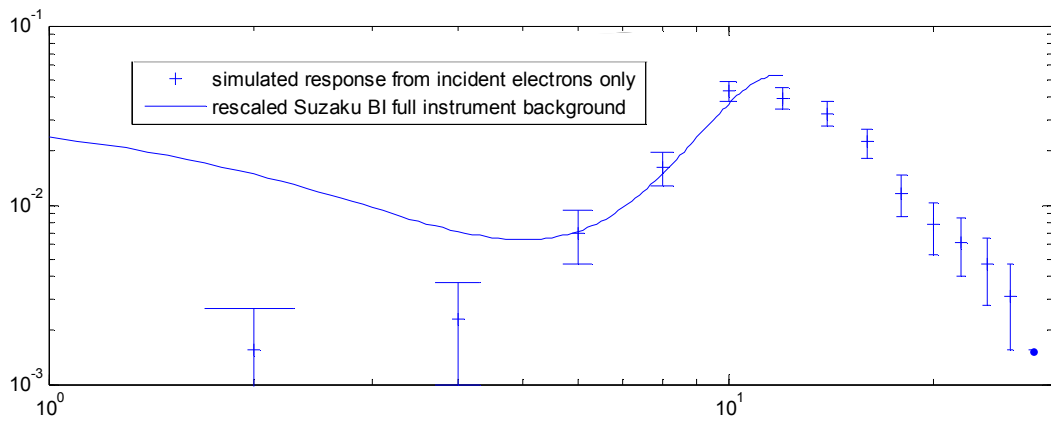
Figure 8. The rescaled response of the Suzaku BI-CCD to incident electrons only, showing the peak in the spectrum at approximately 13 keV relating to a silicon thickness of 45 μm.
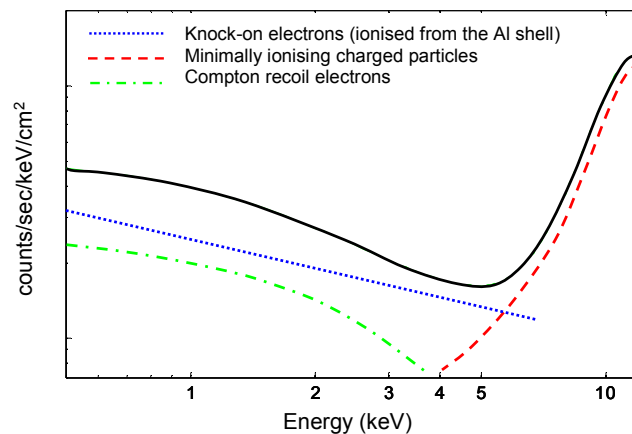
Figure 9. A diagrammatic representation of the three main components forming the instrument background as found in this study, here shown for the Suzaku BI-CCD. The solid line shows the total instrument background. The orbit and detector design determine the relative dominance of each component. Previously shown in [2].

5. CONCLUSIONS

Through the examination of the in-orbit spectra combined with the analysis of the simulation, several new theories on the instrument background can be discussed. Future work involves further simulations to cover the Chandra ACIS and XMM-RGS in order to gain further insight into the results of this study. With future missions in mind, examination of the effects of multi-layered shielding may be of relevance. It may be possible to absorb the knock-on electrons in a succession of thin layers with progressively decreasing electron output. The effects of this structure on the X-ray fluorescence is of great importance and requires future study in order to determine if this would increase or decrease the total effect of the instrument background – a decrease in the spectral continua coupled with an increase in the X-ray fluorescence may be undesirable. It has been shown that this method can be used to reduce X-ray fluorescence [7], but no mention is made of the impact on the flux of knock-on electrons.

Table 4 shows a summary of these results along with brief details of their dependencies on the orbit and device. The spectral continua have been reproduced for the XMM-Newton and Swift missions with the constituent parts of the more complex Suzaku spectra also examined. The results show consistency with the in-orbit data and allow consideration of these factors to be investigated and involved in the planning of future missions.

Table 4. Summary of results from the simulations.

Incident particle	Primary interaction	Orbit dependence	Device dependence
Proton	*Knock-on* electrons travel from the inner surface of the material surrounding the detector. These electrons are detected as X-ray like events at the available surfaces of the detector.	Higher proton flux at higher orbit. Dominating factor.	The structure at the surfaces of the device has a major impact.
Electron	Minimally ionising charged particle depositing energy as it passes through the device giving a peak characteristic to the device thickness.	Greater importance at lower orbit.	The peak will only be significant if near the energy range of interest. Field-free regions cause rejection as signal spreads over many pixels.
Photon	Compton scattered electrons can be generated in the silicon of the device.	Greater importance at lower orbit.	This component scales with device thickness, but is non-dominant compared with the proton effects.

REFERENCES

1. Freyberg, M., J., Briel, U., G., Dennerl, K., Haberl, F., Hartner, G., Pfeffermann, E., Kendziorra, E., Kirsch, M. and Lumb, D., "The EPIC pn-CCD detector aboard XMM-Newton: status of the background calibration," *SPIE* **5165**, 112-122 (2004)
2. Hall, D., Holland, A., and Turner, M., "Modelling instrument background for CCD X-ray spectrometers in space", Proc. SPIE 6686, 66860J (2007)
3. De Luca and Molendi, S., "Studying the cosmic X-ray background with XMM-Newton," *Proc. Symposium 'New Visions of the X-ray Universe in the XMM-Newton and Chandra Era'* (2001).
4. Lumb, D., H., Warwick, R., S., Page, M. and De Luca, A., "X-ray background measurements with XMM-Newton EPIC," *A&A* **389**, 93-105 (2002)
5. Mizuno, T., Kamae, T., Godfrey, G., Handa, T., Thompson, D., J., Lauben, D., Fukazawa, Y. and Ozaki, M., "Cosmic-Ray Background Flux Model Based on a Gamma-Ray Large Area Space Telescope Balloon Flight Engineering Model," *Astrophysical Journal* **614**, 1113–1123 (2004).

6.   Murakami, H., Kitsunezuka, M., Ozaki, M., Dotani, T. and Anada, T., "Origins of the instrument background of the X-ray CCD camera in space studied with Monte Carlo simulation," *Space Telescopes and Instrumentation II: Ultraviolet to Gamma Ray Proceedings* **6266**, 62662Y (2006)

7.   Pfeffermann, E., Friedrich, P., Freyberg, M., Kettenring, G., Krämer, L., Meidinger, N., Predehl, P. and Strüder, L., "Shielding of cosmic ray induced background in CCD detectors for X-ray astronomy," *High-Energy Detectors in Astronomy* **5501**, 304-311 (2004)

8.   H. Yamaguchi, H. Nakajima, K. Koyama, T. G. Tsuru, H. Matsumoto, N. Tawa, H. Tsunemi, K. Hayashida, K. Torii, M. Namiki, H. Katayama, T. Dotani, M. Ozaki, H. Murakami, and E. Miller, Proc. "The background properties of Suzaku/XIS*" SPIE Int. Soc. Opt. Eng.* **6266**, 626642 (2006)